Eur. Phys. J. Spec. Top. (2022) 231:723–734
https://doi.org/10.1140/epjs/s11734-021-00388-3

THE EUROPEAN PHYSICAL JOURNAL SPECIAL TOPICS

Regular Article

Vapor–liquid–solid growth of highly stoichiometric gallium phosphide nanowires on silicon: restoration of chemical balance, congruent sublimation and maximization of band-edge emission

Seyed Ebrahim Hashemi Amiri[1,2], Sunay Turkdogan[1,4], Praneeth Ranga[1], Fan Fan[1], Lin Gan[1,3], and Cun-Zheng Ning[1,3,a]

[1] School of Electrical, Computer, and Energy Engineering, Arizona State University, Tempe, AZ 85287, USA
[2] School of Molecular Sciences, Arizona State University, Tempe, AZ 85287, USA
[3] *Present Address:* Department of Electronic Engineering, Tsinghua University, Beijing, China
[4] Departments of Electrical and Electronics Engineering and Energy Systems Engineering, Faculty of Engineering, University of Yalova, Yalova 77002, Turkey

Received 12 August 2021 / Accepted 13 December 2021 / Published online 3 January 2022

Abstract Growth of high quality III–V compound nanowires using simple chemical vapor deposition method with safe, inexpensive precursors is extremely important for a wide range of applications from solar cells, detectors, to light emitting devices. However, the most-often used deposition approach using compound powers suffers from incongruent sublimation of group III and V elements, leading to premature exhaust of group V elements and eventually to defective, non-stoichiometric nanowires with poor electronic and optical properties. In this paper, we report new results of our efforts in resolving these challenges using as an example the growth of GaP nanowires, an important widegap semiconductor. Our results reveal fascinating roles played by the elemental P source in addition to GaP powder such as restoration of chemical balance, inhabit of the incongruent sublimation of GaP, and the growth of highly stoichiometric GaP NWs with high optical quality and maximized band edge emission. The effects of growth parameters such as growth time, orientations of silicon substrate, growth temperature, and precursor combinations are studied and correlated to stoichiometry of NWs, and to the existence and degree of deep defect states and band edge emission. Our study sheds new light onto the important interplays among all these important factors. Our strategy is not only important for the growth of GaP nanowires on silicon but also for other III–V compounds as well using CVD and inexpensive compound powder sources.

1 Introduction

Semiconductor nanowires of group III–V and II–VI compounds and their alloys have been studied extensively for a wide variety of photonic applications over the last two decades [1–4]. As an important III–V compound, Gallium Phosphide (GaP) nanowires (NWs) have attracted a great deal of attention among III–V materials, especially due to its role as an alloy partner with InP or GaAs for a wide array of optoelectronic device applications [5–7] such as light emitting diodes (LEDs) [8], solar cells [9], photoelectrochemical cells [10], etc. GaP NWs have been synthesized using various methods such as laser ablation [11], metal organic vapor phase epitaxy (MOVPE) [12], Molecular beam epitaxy (MBE) [13] surfactant-free solution–liquid–solid (SLS) synthetic method. [14] However, the growth of oxide-free Ga-compounds such as GaP NWs via vapor phase transport method [7,15–18] has shown to be difficult, mostly due to formation of stable oxide species such as Ga_2O_3, and $GaPO_4$ that are thermodynamically easy to incorporate into GaP NWs, resulting in poor optical quality. [15] For applications where the low cost is more important such as solar cells, the simple chemical vapor deposition (CVD) with low-cost precursor materials such as GaP power is preferred. However, the effect of large difference in sublimation rates of group III and V elements are known to be a key issue for the growth of III–V materials such as InSb [19,20], GaSb [21], InP [22,23], GaAs [24,25], GaP [26,27], InAs [28] , etc. Such incongruent sublimation leads to stoichiometrically imbalance in the final compounds. One of the important issues is the lack of pressure–temperature–composition (P–T–X) equilibrium phase diagram for a sealed system with simultaneous presence of vapor, liquid and solid phases. [29,30] Therefore, it is quite a challenge to find an ideal growth condition to maintain stoichiometric growth using binary GaP precur-

[a] e-mail: cning@tsinghua.edu.cn (corresponding author)

sor. In another word, the whole 3D phase space must be explored to determine suitable (P, T, X) values to grow stoichiometric NWs. The vacancies and interstitial atoms associated with non-stoichiometry have severe adverse effects on the optical and electrical the properties [30–33]: for example, small deviations from stoichiometry in GaP can have strong impacts on luminescent efficiency [34,35]. Few study exists in literature on the effects of deviation from stoichiometry on optical properties of GaP. Also, there is a lack of systematic study of parametric dependent growth and understanding of non-stoichiometry. In binary semiconductors such as GaP, deviation from stoichiometry can cause vacancies (V_{Ga}, V_P), antisites (P_{Ga}, Ga_P) and self-interstitials (P_i, Ga_i), leading to the degradation of optical quality and device performance [36]. Formation of such point defects in bulk GaP has been studied from both computational and experimental points of view [38–41]. Presence of such defect-related deep levels near the band edge has been previously reported in other direct bandgap ZnO [42] and ZnSe [43] NWs using their photoluminescence (PL) characteristics, but there have been few reports [44,45] on PL study of defect-induced emission in GaP NWs. In this paper, we present results of our systematic study of a low-cost vapor phase CVD technique for the growth of GaP NWs based on vapor–liquid–solid (VLS). The main objective of this paper is to study the effects of growth conditions, substrates and precursors on stoichiometry of GaP NWs and to establish a link between stoichiometry to the intensity ratio of band edge emission to defect emission. Our study involved systematic materials growth experiments under various conditions and the corresponding optical and material characterizations. Such study allows the establishment of a growth strategy for producing high quality GaP NWs based on a simple, inexpensive approach. Our systematic growth studies show that elemental phosphorous is necessary in addition to binary GaP precursor to replenish P deficiency and to produce highly stoichiometric NWs. In particular, we examine the growth conditions to produce maximized BE to DE intensity ratio, both as an important requirement for many photonic applications, and as a direct and simple indication of stoichiometry and crystal quality of grown NWs.

2 Experimental details

2.1 Sample synthesis

Our growth experiment was carried out in a horizontal low-pressure CVD setup. Schematic illustration of growth set up and procedure is provided in Supporting Information (Fig. S1). GaP NWs were grown on Si substrates coated with a nominal Au thickness of ∼ 1–10 nm as the catalyst for VLS growth, via sputter deposition at room temperature. The Au-coated substrate was placed at downstream side of a single zone furnace where temperature ranges from 720 to 800 °C. Growth at lower temperatures than 720 °C is shown to have high oxygen content in NWs (Fig. S2). As the source materials, ball milled high purity GaP (99.999% Alfa Aesar), Gallium metal and red Phosphorous powder (≥ 99.99% Sigma Aldrich) were used. Ar + 5% H_2 with flow rate of 40-45 sccm (standard cubic centimeter per minute) was used as carrier gas and the pressure of the reactor was kept constant around ∼ 5 Torr using a mechanical pump attached to the capacitance manometers. Prior to growth, the ball-milled GaP powder was placed in the middle of the furnace where temperature is maximum. A magnetic manipulator was utilized to position the red phosphorous, upstream from the GaP precursor, outside of the furnace heating zone (see Fig. S1). In different experiments, Ga source was also placed in a separate boat upstream of the GaP boat. The system was purged for 1 h under 300 sccm flow rate of carrier gas to purge excessive oxygen, CO_2 and water molecules inside the furnace tube. After the furnace reached the target temperature of 1000 °C with a ramp up rate of 42 °C/min, the red phosphorus boat was pushed inside the furnace using a magnetic manipulator where the temperature was 400–450 °C. After a certain period of growth time (7 to 45 min) the system was naturally cooled down to room temperature. To study the effects of various precursors, experiments were carried out with pure GaP, GaP with P, and GaP with Ga as the source materials.

2.2 Material characterization

The morphology of the as grown samples was studied using a field emission scanning electron microscope (FE-SEM, XL-30). Elemental composition of NWs was determined by energy dispersive X-ray spectroscopy (EDS). High resolution transmission electron microscopy (HRTEM) images of NWs were obtained using an aberration-corrected Titan 300/80 (FEI) microscope at operating voltage of 300 keV. To investigate the optical properties of the NWs, photoluminescence (PL) measurements were performed at room temperature using an Nd: YLF laser (Spectra Physics, λ = 349 nm, repetition rate of 10 Hz, pulse width of 5 ns) as the excitation source. X-ray Diffraction (XRD, PANalytical X'Pert PRO MRD, Cu Kα, wavelength λ = 1.5405 Å) was also used to determine the crystal phase structure of the NWs. To further evaluate the long-range order crystallinity, the Raman measurement was carried out using a 150 mW Coherent Sapphire single frequency laser with a wavelength of 532 nm. Details are presented in SI.

3 Results and discussion

3.1 Growth of stoichiometric GaP nanowires: effects of source materials

Our choice of source materials is guided by simplicity, safety, low cost, and most importantly the ability to lead to high quality material. One of the greatest

advantages of the low-cost CVD approach is to be able to use the same compound powder as source material to grow NWs of the same material. As presented in SI, our growth experiments using pure GaP source lead to GaP NWs with a poor stoichiometry, due to a much higher sublimation of P than Ga atoms and premature exhaustion of P. Initially such high P sublimation rate leads to excess P in gas phase and in the final grown NWs. But during the later stage of growth, the reduced availability of P in the source boat leads to less availability of P and eventually the deficiency of P in the grown NWs for longer time growth, as shown in Fig. S3. The EDS measurement after 45 min of growth left the source with a P to Ga ratio of ~ 11 to 59, with 29% of oxygen incorporation. To have a complete picture of the effects of source materials, we tried to introduce Ga in addition to GaP as source material. The EDS analysis after 15 min of growth was shown in Fig. S4a and b. The addition of Ga apparently exacerbated the incongruent sublimation of Ga and P. The source boat P to Ga ratio was even more asymmetric in favoring a faster P sublimation. Interestingly, the NWs have a higher P (Ga/P = 47.14/52.86) after the first 15 min growth due to the enhanced P availability in the initial stage of growth.

To understand the situation, we consider the difference in partial vapor pressures of Ga and P above GaP boat and how it relates to the chemical potential difference ($\Delta\mu$) between vapor and solid phases. It is known for many III–V compounds including GaP that above the congruent sublimation temperature ($T_{cs} = 571$ °C for GaP), GaP loses phosphorous from the surface, preferentially over Ga. [46] For the sublimed GaP, the phosphorous dimers (P_2) and tetramers (P_4) are the common molecular compounds that have higher equilibrium partial pressure than that of the Ga element, above the T_{cs}. [27,47] The issue of stoichiometric asymmetry also existed in the conventional thin film growth of III–V compounds. The effect of maintaining a P-rich environment during MOVPE and MBE growth of GaP thin films has been widely explored . [48–52] The incorporation of impurities such as Ga and P lattice vacancies is known to result in surface imperfection on epitaxially grown GaP films. Providing excess phosphorus precursor flow is necessary in surface reconstruction of GaP which usually occurs due to thermal decomposition of GaP and subsequent Ga, and P desorption. Leys et al. have demonstrated the effect of P-rich environment in enhancing the stoichiometry of the surface during growth and enabling smooth epitaxial GaP layers. [53] In addition, on the supercritical fluid–liquid–solid (SFLS) synthesis of GaP NWs, Davidson et al. have shown the necessity for excess phosphorous source to achieve a balanced stoichiometry [54]. While these studies are important in addressing the issue of different vapor pressures of group III and V elements in conventional thin film growth, as we mentioned earlier, our preference for the use of GaP power in the low cost growth of nanowires in a simple CVD necessitate an independent study of this issue reported here.

In general, there are two ways to prevent the non-stoichiometric sublimation of group III and V species. One way is to determine the sublimation phase diagram in P–T space to maintain GaP source boat always under congruent conditions. This requires numerous experiments under different P–T combinations to determine such phase diagram and becomes impractical. Additionally, the likely required low sublimation rate would lead to extremely slow growth of NWs and become impractical for many low-cost applications. Our goal is to find an alternative to maintain a highly positive chemical potential for P in gas phase above source boat, since the chemical potential of P in gas phase is normally very low when pure GaP is used. Since the growth process occurs under the constant carrier gas flow rate, total pressure of growth chamber and evaporation temperature are kept constant, thus the system is thermodynamically under quasi-equilibrium condition. The condition during the sublimation process under constant temperature and pressure is written as follows:

$$\mathrm{GaP\,(solid)} \overset{quasi-equilibrium}{\Longleftrightarrow} \mathrm{Ga\ (liquid/gas)} + \uparrow \mathrm{P\ (gas)}. \tag{1}$$

The sublimation reaction can be explained by different levels of chemical potential [55,56] obtained at various growth conditions. Let μ_j^i be the chemical potential of species i (P or Ga) in phase j. Hence, $\Delta\mu = \mu_g^P - \mu_s^P$ is the difference in chemical potential of P in the gas and solid phase. The $\Delta\mu$ for the growth using pure GaP source compared with excess P source condition is given by;

$$\text{Pure GaP;} \quad \mu_s^P > \mu_g^P, \text{or } \Delta\mu < 0, \tag{2}$$

$$\text{GaP and P;} \quad \mu_g^P > \mu_s^P, \text{or } \Delta\mu > 0. \tag{3}$$

Therefore, by increasing the partial vapor pressure of phosphorous in the growth system by providing an additional P source the $\Delta\mu$ becomes a positive term, leading to the inhibited sublimation of P from the GaP source.

Experiments were performed to verify the above understanding with an additional elemental P added to the GaP precursor to replenish the deficiency of P after the initial phase of growth. Indeed, our examination of source boat and grown NWs after a 15-min growth in the presence of additional elemental P shows a more congruent sublimation. Figure S4c,d show highly stoichiometric NWs and remaining GaP in the boat in contrast to the growth with pure GaP source or with GaP and Ga source. More importantly, this approach also led to very congruent sublimation of GaP from the source boat and a stoichiometric GaP NWs for long time growth, as shown in Fig. 1c for a 45 min growth. A top view of representative SEM image of GaP NWs grown at 800 °C for 45 min using both red-P and GaP source materials on a Si (100) substrate is shown in Fig. 1a. Inset (right) of Fig. 1c shows a GaP NW dis-

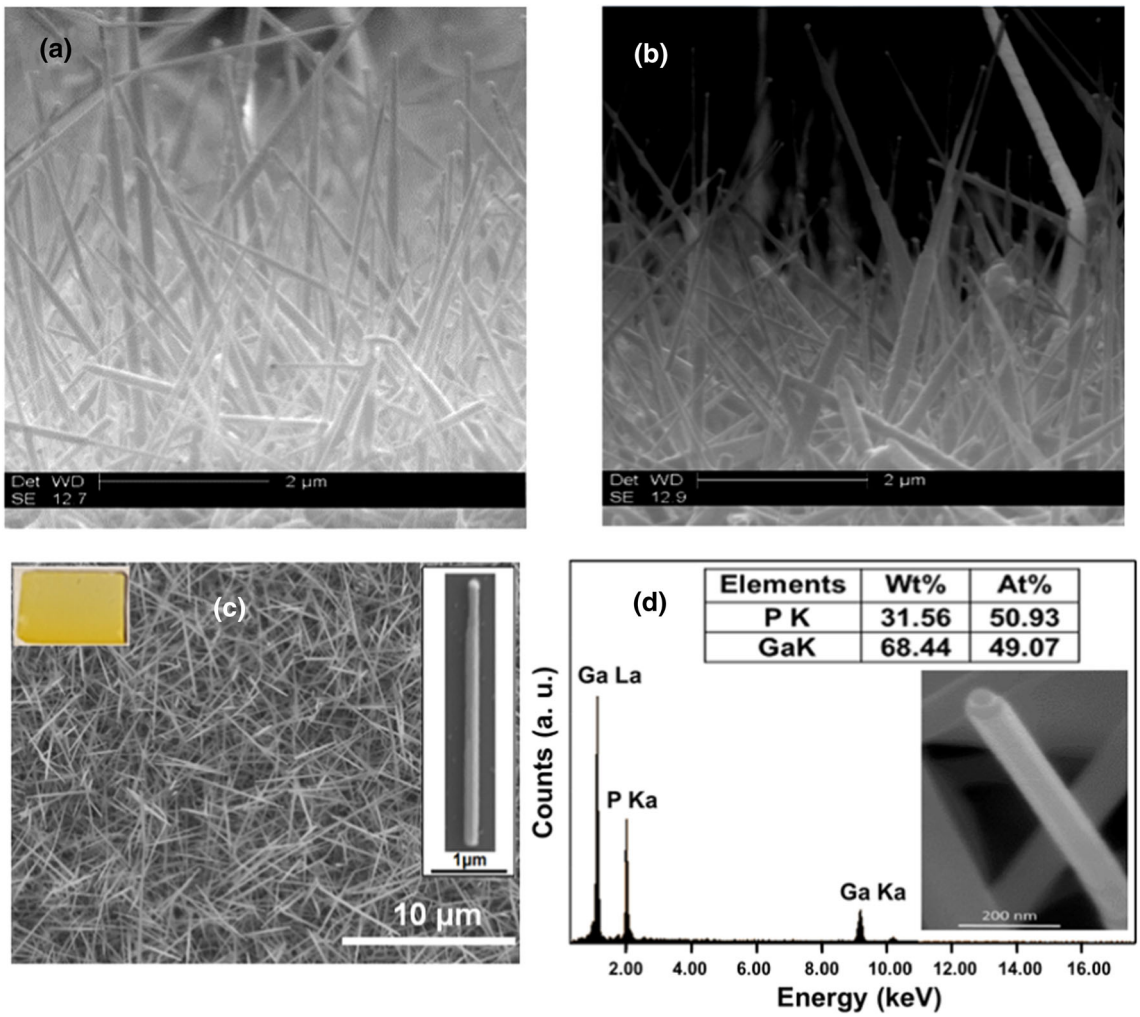

Fig. 1 Side views of SEM micrograph of GaP NWs grown on Si (111) (**a**) and Si (100) (**b**) substrate after 15 min of growth; **c** shows the top view of SEM image after 45 min of growth on a larger scale with insets showing a real color image of as grown sample (top left) and an enlarged view of a single NW with Au tip, dispersed on glass (right); **d** A typical EDS spectrum of individual wires for the growth time of 45 min with weight and atomic compositions shown in the inset table, indicating high stoichiometric symmetry for a faceted NW with Au catalyst shown in the inset

persed on a glass with a uniform body and slight necking near the Au tip. The top left inset of Fig. 1c shows a photograph of the whole substrate under room lighting (yellow color), showing the large-scale uniformity over the substrate of 10 by 15 mm in size. The energy-dispersive X-ray spectroscopy (EDS) analysis (Fig. 1d) on the body of GaP NWs grown using GaP+P source shows the Ga:P atomic ratio to be 1.00:1.02, with only $\sim$ 2% deviation from stoichiometry. A high magnification SEM image of the corresponding NW shows its faceted morphology (inset of Fig. 1d). Our extensive growth experiments established that the combined GaP and P source material combination is ideal for the growth of high quality and high stoichiometric GaP NWs. In the following, our study will be focused on the growth with the combined source materials of GaP and P.

3.2 Structural characterization

In order to study the crystal structure of GaP NWs grown using GaP+P source, XRD measurements with X-ray source of Cu Kα were carried out. For both samples grown on Si (100) and Si (111) three main diffraction peaks were observed at 2θ values of 28.37°, 47.24°, and 55.79°corresponding to (111), (220), and (311) crystallographic planes of zinc blende (ZB) GaP, respectively (Fig. 2a). From normalized XRD spectra both samples show a sharp (111) peak, where the GaP NWs grown on Si (111) show a more dominate peak along [111] direction.

Furthermore, we have further examined the crystal quality of GaP NWs using Raman spectroscopy (see SI for measurement details) in which the Raman shift related to the inelastic scattering reveals the informa-

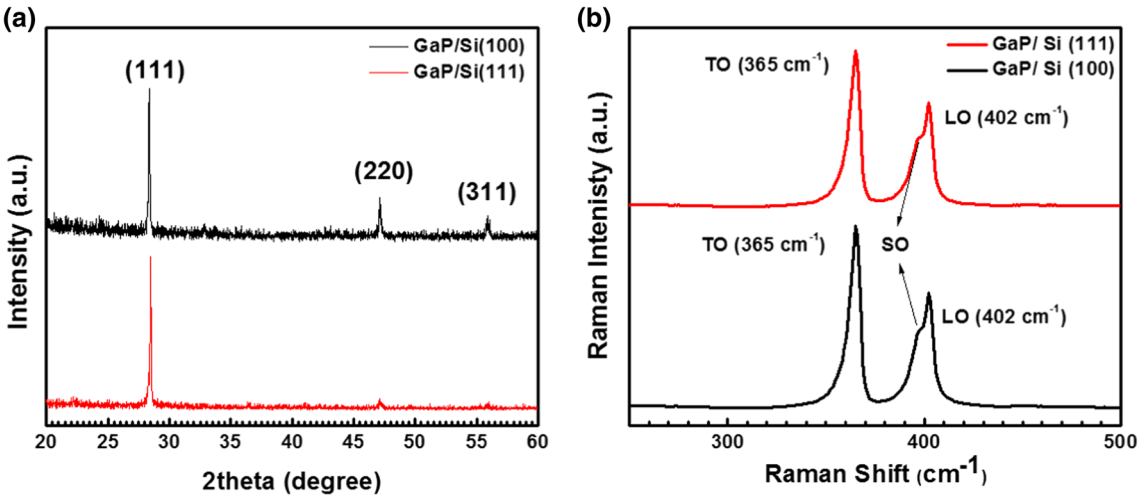

Fig. 2 **a** XRD and **b** Raman spectra of GaP NWs grown on Si (100) and (111) substrates using GaP+P source. The first-order TO ($365\,cm^{-1}$) and LO ($402\,cm^{-1}$) are downshifted compared to the bulk GaP with (111) orientation by 2 and $1\,cm^{-1}$, respectively. Presence of surface optical (SO) modes is attributed to the surface scattered phonons due to extremely large surface of GaP NWs or amorphous oxide layer

tion of the crystal structures [57]. The Raman scattering spectra of the GaP NWs are presented in Fig. 2b at room temperature for two different samples grown on Si (111) and Si (100). Two phonon modes, the transverse optical (TO) and longitudinal optical (LO) phonon modes appear at around 365 and $402\,cm^{-1}$, respectively. These values are in good agreement with the reported bulk values for GaP [58] and the numbers obtained for single crystal GaP wafers (Table S1).

The FWHM of TO mode is 6.04 and $5.98\,cm^{-1}$ for GaP NWs grown on Si (100) and Si (111), respectively. Similarly, the linewidth for LO mode is 4.39 and $4.01\,cm^{-1}$, respectively. For comparison, we also measured the linewidth of single crystal GaP wafer and obtained FWHM of $7.88\,cm^{-1}$ for TO mode and $5.29\,cm^{-1}$ for LO mode. These Raman linewidths indicate a very good crystal quality for NWs and slightly better crystallinity for the sample grown on Si (111). The slight downshift of both TO and LO modes might be because of an excess of phosphorus (as interstitial or antisites) in the GaP resulting in slight lattice distortion [59,60]. The TO/LO intensity ratio for NWs grown on Si (100) and Si (111) is 1.55 and 1.48, respectively. It is known that TO/LO intensity ratio is directly correlated with the concentration of defects [61]. This slight difference is presumably due to different concentration of intrinsic point defects in two samples. For the single crystal GaP wafer this ratio is below 1 which is indicative of smaller concentration of defects. The shoulder on the LO peak of GaP for both samples is related to surface optical (SO) phonons due to existence of a surface or an interface of amorphous surface oxide in core-shell GaP NWs [62]. The SO modes in NWs appear due to extremely large surface of GaP NWs compared to bulk GaP [63–66] which is not observed for GaP bulk as shown in Fig. S6. The absence of SO mode for wafer indicated that the physics behind Raman scattering of one-dimensional nanostructures such as NWs can be different from that of bulk which is due to the fact that Raman features in NWs are angular dependent due to their highly anisotropic shape [67].

The bright-field (BF) TEM images of a typical VLS-grown GaP NW grown on Si (111) substrate for 15 min is shown in Fig. 3a. Formation of segments of different contrast (Fig. 3a, c) is attributed to coherent twinning segments, also called twining superlattice (TSL), with different rotational twins. HRTEM of an individual NW showed a high density of stacking faults (SF) and twinning defects (Fig. 3b). The ABCABC stacking of atomic planes are also indicative of cubic ZB structure. Shown in the right side of Fig. 3b are the selected-area electron diffraction (SAED) pattern taken from two adjacent segments separated with a thin multiatomic layer of microtwins (MTs) making a rotation angle of 141° when viewed from $< \bar{1}10 >$ zone axis (Fig. 3e). From the interplanar spacing between parallel lattice fringes, the lattice constant is calculated to be 0.314 nm which corresponds well to the (111) interlayer spacing of bulk ZB GaP, thus confirming $< 111 >$ as the growth direction. The indexed double-spot superimposed pattern obtained by fast Fourier transform (FFT) shown in Fig. 3d corresponds to SAED pattern of ZB twinning sections of GaP NWs. Both patterns have a twofold symmetry along $< \bar{1}10 >$ zone axis that have a rotation of $\sim 70°$ (or 110°) with respect to each other. Formation of such quasiperiodic twinning segments within entire body of NW corresponds to intermittent rotational twins introduced by SFs along $< 111 >$ growth direction. Presence of an amorphous layer outside of both NW body and Au–Ga–P alloy droplet is due to existence of Ga–P–O compounds such as $GaPO_4$ and Ga_2O_3 that are formed in ambient environment prior to transferring of the NWs onto TEM grid (Fig. 3f).

The exact mechanism of formation of rotated twins is not yet fully understood. However, their dependence on growth temperature, diameter of NW and dopants has

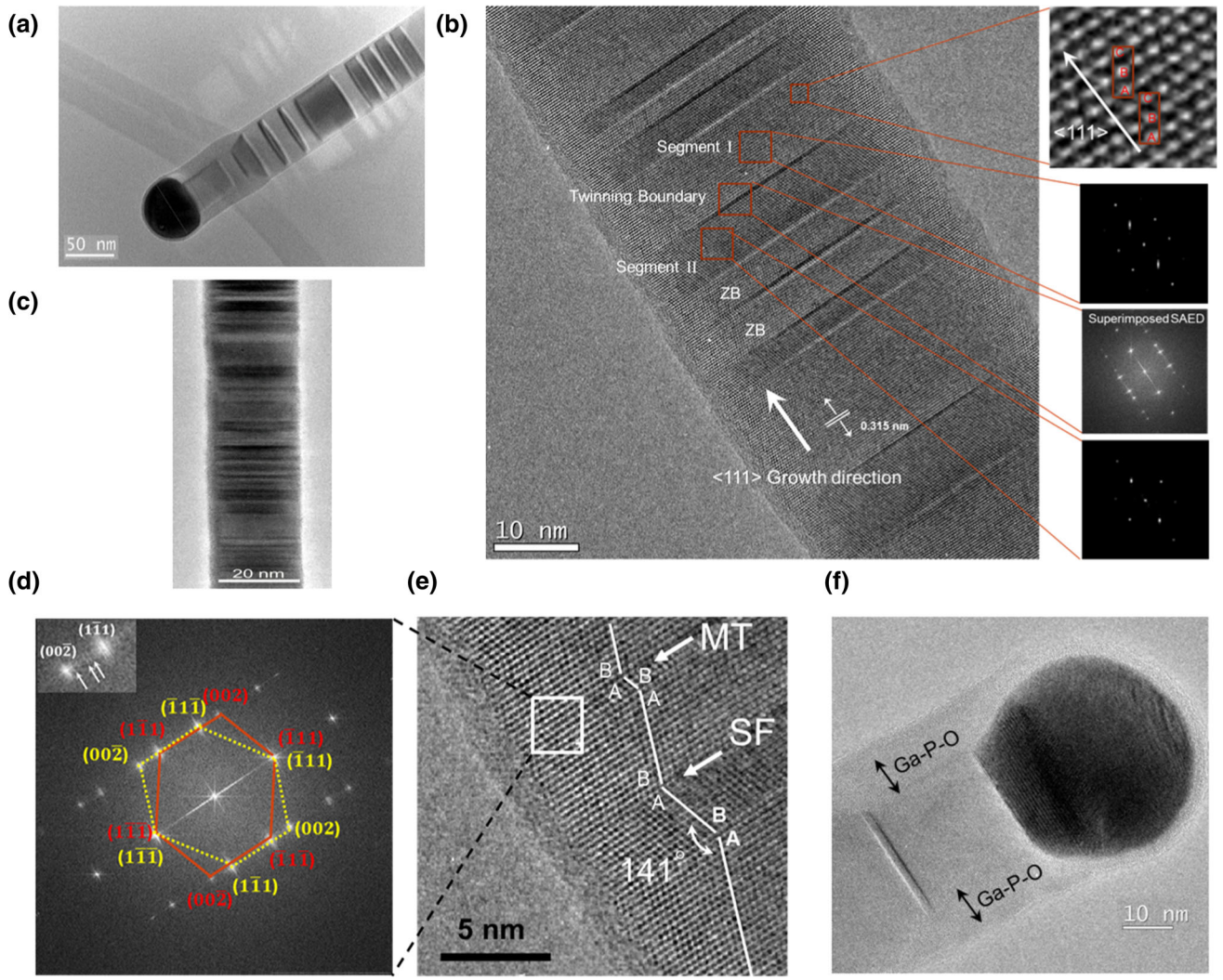

Fig. 3 TEM study of GaP NWs grown under P rich condition. **a** Bright field TEM image taken from the NW of 50 nm diameter with evident TSL onset showing transition from single-crystal growth to coherent twinning growth. **b** high-resolution (HRTEM) image of quasiperiodic TSL along [$\bar{1}$10] zone axis with ABCABC stacking, for each segment, attributed to the normal ZB planar sequence with $< 111 >$ growth direction. The associated FFT images are taken from two adjacent segments and twin boundary, in which the diffraction spots correspond to the (111) planes perpendicular to the growth direction. **c** Formation of planar defects such as SFs and twin-planes within entire body of a GaP NW with the observed smallest diameter of 20 nm. **d** Indexed double spot FFT pattern (two superimposed pattern) along [$\bar{1}$10] zone axis pattern. Inset with some white arrows represents some of the spots diffracted from the TSL. **e** HRTEM image of twin segments with SFs and MTs formed at the boundaries. **f** Amorphous layer outside of both NW body and Au–Ga–P alloy droplet is due to formation of Ga–P–O compounds such as $GaPO_4$ and Ga_2O_3

been studied [68,69]. It has been reported that periodic array of twin boundaries forming a superlattice can result in formation of minibands due to periodic electron scattering [70].

3.3 Optical characterization

Photoluminescence study was performed using an Nd:YLF UV-laser (349 nm) as the excitation source to study the optical properties of NWs. Room temperature PL spectra of as-grown GaP NWs showed (see Fig. 4) that there are two dominant characteristics peaks; a narrow band edge (BE) emission at 556 nm attributed to the transition of indirect bandgap, Γ_V-to-X_C, and a broad band peak at 690–720 nm, typically seen in GaP and attributed to deep defect related recombination. To examine the emission features of NWs, we performed pump-power dependent PL measurements, as shown in Fig. 4b. As we see there, the relative emission intensities change with decrease in defect emission (DE) and increase in BE, consistent with the assignment of 690–720 nm range as the DE band. Due to the smaller density of states in DE band,

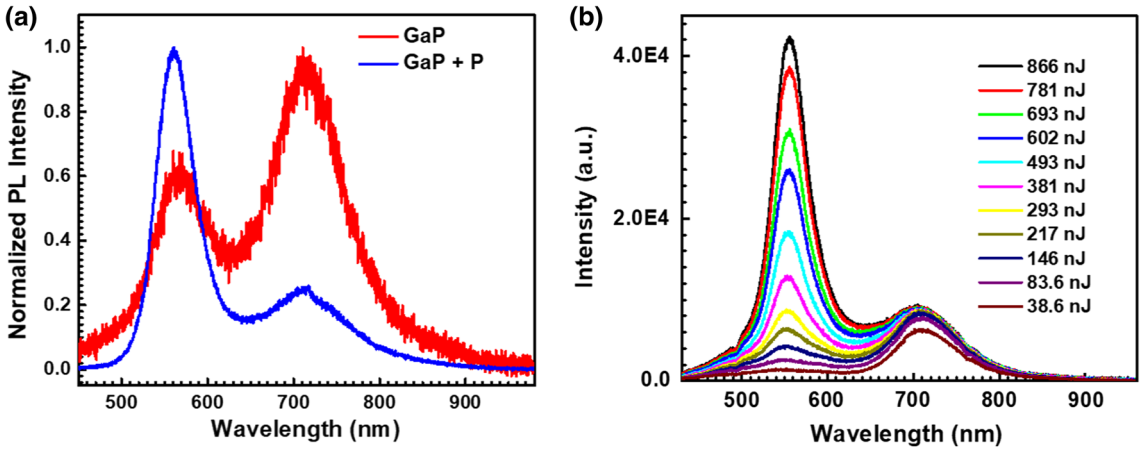

Fig. 4 Photoluminescence (PL) of GaP NWs grown at 800 °C on Si (111) for 45 min with Au thickness of 1–1.5 nm. **a** Comparison of normalized PL spectra at pumping energy of 493 nJ for NWs grown using pure GaP source and under excess P condition; **b** PL spectra for GaP NWs at various pumping levels showing increasing BE emission relative to defect emission with increased pumping

the DE band is quickly filled up with the increase in pumping, resulting more population of BE states. To relate the material quality with relative BE–DE intensities, we compared PL from sample grown using pure GaP source and that grown using the combined GaP and P sources, as shown in Fig. 4a. It is clear that the less stoichiometric NWs grown in the former case show much stronger DE emission than the stoichiometric NWs of latter case. This further validates our proposed approach of using a combined GaP and P sources as precursors for the growth of high quality NWs. Presence of such native defect was also observed in PL spectrum obtained from single-crystal GaP wafer, despite their high crystal quality (Fig. S8) which will be shown later in comparison with the as our grown NW samples. The integrated BE to DE (IBE/IDE) ratio to is the more precise way to gauge how much the BE predominates over DE and will be examined more in the following. The IBE/IDE ratio shows a ~ 3 fold increase for growth with additional P (from 0.37 with pure GaP source to 1.13 with GaP and P sources). This comparison shows that the P-deficiency contributes significantly to the DE. Quantitatively, the threefold increase of IBE/IDE ratio corresponds to an improvement of stoichiometry of about 5.5% (from 6.15% to 0.66%). In order to establish a correlation between the stoichiometry and IBE/IDE intensity ratio we have measured the PL for GaP NW samples grown under various experimental conditions including two different orientations of Si substrate, growth temperature, growth time, etc and the results are summarized in Fig. 5 and in Table S2.

The comparison of IBE to EDE ratio (IBE/IDE) for 9 different samples shown in Fig. 5 is based measurement of PL on as-grown samples at the equal pumping energy of 493 nJ. First the Lorentzian fitting was performed for both BE (in the range of 460–650 nm) and DE (in the wavelength range of 550–850 nm), respectively. As measure of stoichiometry, P/Ga ratio was obtained from EDS results of all samples, transferred via contact printing [71] from the original substrates onto fresh quartz substrate (Table S2). To measure uniformity, 6 NWs were measured from each of 9 samples, as presented by 6 data points along each horizontal line in Fig. 5. Since PL measurement was performed on as-grown samples with a micron-size resolution, all 6 SEM measurements from a given sample corresponds to a single IBE/IDE ratio. In Fig. 5, 9 samples are divided into 3 groups based on growth temperature and time. A few observations can be made from Fig. 5: First, NWs with high stoichiometric symmetry (P/Ga$\sim$ 1) shows higher IBE/IDE ratio. The best examples are samples 6 and 7, showing the highest IBE/IDE ratio of larger than 2.5. Second, samples grown for shorter time (15 min, samples 6 and 7) have higher IBE/IDE ratio than longer time (45 min, samples 1 and 2) under the same growth conditions. This is likely due to the fact that smaller wires grown for shorter time are less likely to incorporate into defects. It is also interesting to note that there is no apparent difference in stoichiometry between the two groups of wires. Therefore, the additional defects incorporated into samples 1 and 2 are likely to be stoichiometric. Third, NWs grown with thinner layer of Au are more stoichiometric and have stronger BE (higher IBE/IDE ratio), as can be clearly seen by comparing samples 1 through 5, as Au is increased from 1–1.5 nm, 2–3 nm, to 6–9 nm. Another observation is that there is little difference between substrate orientations (Si (100) vs. Si (111)) in terms of stoichiometry or IBE/IDE ratio. We also observe that in general, higher growth temperature leads to better stoichiometry and better BE. The ideal growth window of temperature is in the range of 720–800 °C. Within the ideal temperature window, higher temperature does not necessarily lead to better material quality. An example is provided by comparing sample 9 grown at 720 °C with sample 2 grown at 800 °C, where lower temperature gives higher IBE/IDE ratio. It is also worth noting that there is a

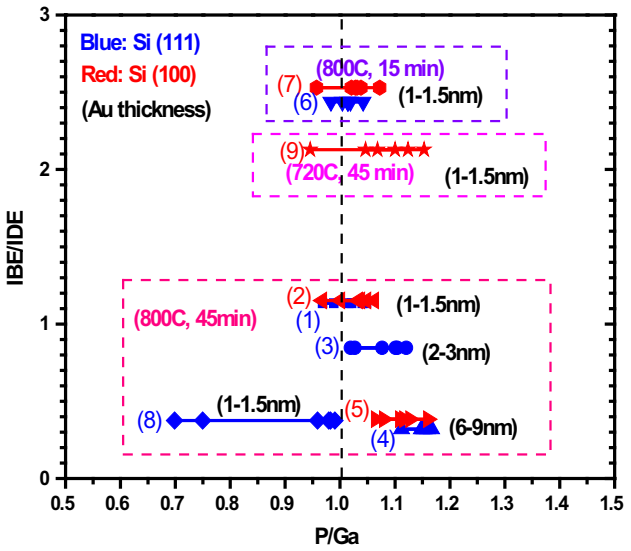

Fig. 5 Relationship between IBE/IDE ratio and stoichiometry and IBE/IDE for various GaP samples grown under different conditions. Deviation from stoichiometry (P/Ga = 1) is determined from EDS analysis of single NWs/spots. The IBE/IDE intensity ratios are obtained based on integration of Lorentzian fitting of PL spectra (under identical PL pumping energy of 493 nJ) within identical range of 460–650 nm for BE and 550–850 nm for DE peaks, respectively. Samples are divided into three groups based on the growth conditions (dashed boxes). The numbers in the parentheses in front of data set indicate the samples numbers used in SI Table S2. The black numbers with unit of nm indicates the thickness of Au catalyst before the growth. All samples were grown using GaP + P as recipe except sample 8, which was grown using GaP only

change of DE central wavelength from 690 nm at 720 °C to 718 nm at 800 °C (see Table S2 and Fig. S7). Another exception to the above observations is sample 8, which was grown under otherwise the same conditions as sample 1. The poor stoichiometry and low IBE/IDE ratio are results of growth with pure GaP source without additional P, while all other 8 samples were all grown with GaP+P source materials. This further verifies the key result of this paper that GaP together with P provides an ideal source combination. We believe that such systematic understanding could be utilized to guide the growth of high quality GaP NWs.

To gain more quantitative information about the spectroscopic features of NWs, we examined pumping power dependence of IBE, IDE, IBE/IDE ratio, and linewidths of BE and DE of two of our samples grown on Si (100) and Si (111) and compared such features with those of commercial GaP wafer, as shown in Fig. 6 for two of our samples (samples 6 and 7 shown in Fig. 5). The three samples (sample 6, 7 and wafer) were pumped with pumping energy from 217 nJ to 866 nJ and their PL spectra are shown in Fig. S8a–c. The details of Lorentzian fitting are shown in Fig. S8d–f and in Table S3. For this comparison, it is important to note that the reflection from NWs samples is very different from the flat GaP wafer. The reflectivity of the GaP wafer was estimated to be R = 51.15% from Fresnel's equation for an incident laser light angle of 30°. The pumping intensity of GaP wafer was therefore scaled by (1-R). Such difference while affecting an absolute comparison between the wafer and NW samples, does not affect the slopes of quantities that we plot on log–log scale in Fig. 6a–c. First, we notice that the IBE of GaP wafer shows a strongly super-linear increase (with a scaling index larger than 2) with pumping, mostly as a result of increased penetration depth of pumping beam into a very thick wafer. The IBE from both NW samples shows a slightly sublinear increase with a scaling index close to but smaller than 1. The DE for all three samples shows the same sub-linear increase, as the DE bands are filled up with increasing pump. The IBE/IDE ratio reflects mostly the behavior of IBE, since IDE is similar for all of them. The linewidth comparison shown in Fig. 6d is more interesting. The linewidths for all DE bands increase with pumping, while linewidths for BE of NWs decrease and that for the wafer stays practically constant. The increase of DE linewidth is a result of filling of DE states of wider range as pumping increase. The absence of linewidth increase for wafer is an indication that there are little shallow defect states as a result of high quality wafer. The decrease of BE linewidth for NW samples indicates a saturation of shallow defect states in NWs with pumping, as the excited carriers populate increasingly more and more states in the continuum bands. The larger BE linewidth of NWs than that of wafer indicates existence of shallow defect states, most likely related to the surface states and other twinning defects as seen in the HRTEM analysis. Thus, the linewidth approaches the more intrinsic linewidth determined by the band structure, as in the case of wafer.

The DE band observed in PL spectrum is often attributed to structural defects such as stacking faults, twins [72,73], and non-stoichiometric point defects [74,75], that introduce deep electronic levels within the band gap. The density functional theory (DFT) calculation by Höglund et al. [41] for local density approximation [76] of native defect states in GaP has shown that the stable charge states which have neither electrons in conduction band nor holes in valence band are primarily vacancies and antisites rather than interstitial species, mostly due to their relatively lower formation energy [41,76]. Formation of localized energy levels within the band gap associated with point defects that combine to form donor–acceptor pairs seems to be responsible for electronic transition of 1.7–1.75 eV for GaP NWs. It is reported in GaP, the intrinsic point defects introduced during the growth under excess P condition, are predominantly P_{Ga}^{+2} and V_{Ga}^{-3} [41]. However, we have observed the DE at 690–720 nm (or 1.8–1.72 eV) for all the samples grown near stoichiometric concentration using vapor phase method using Ga, GaP + Ga, and GaP + P sources. Formation of these DE levels could be attributed to the shallow acceptor level of V_{Ga} (at E_c–1.7 eV) or donor level of P_{Ga} (at E_c–0.6 eV) [75]. The location of Fermi-level strongly depends on the concen-

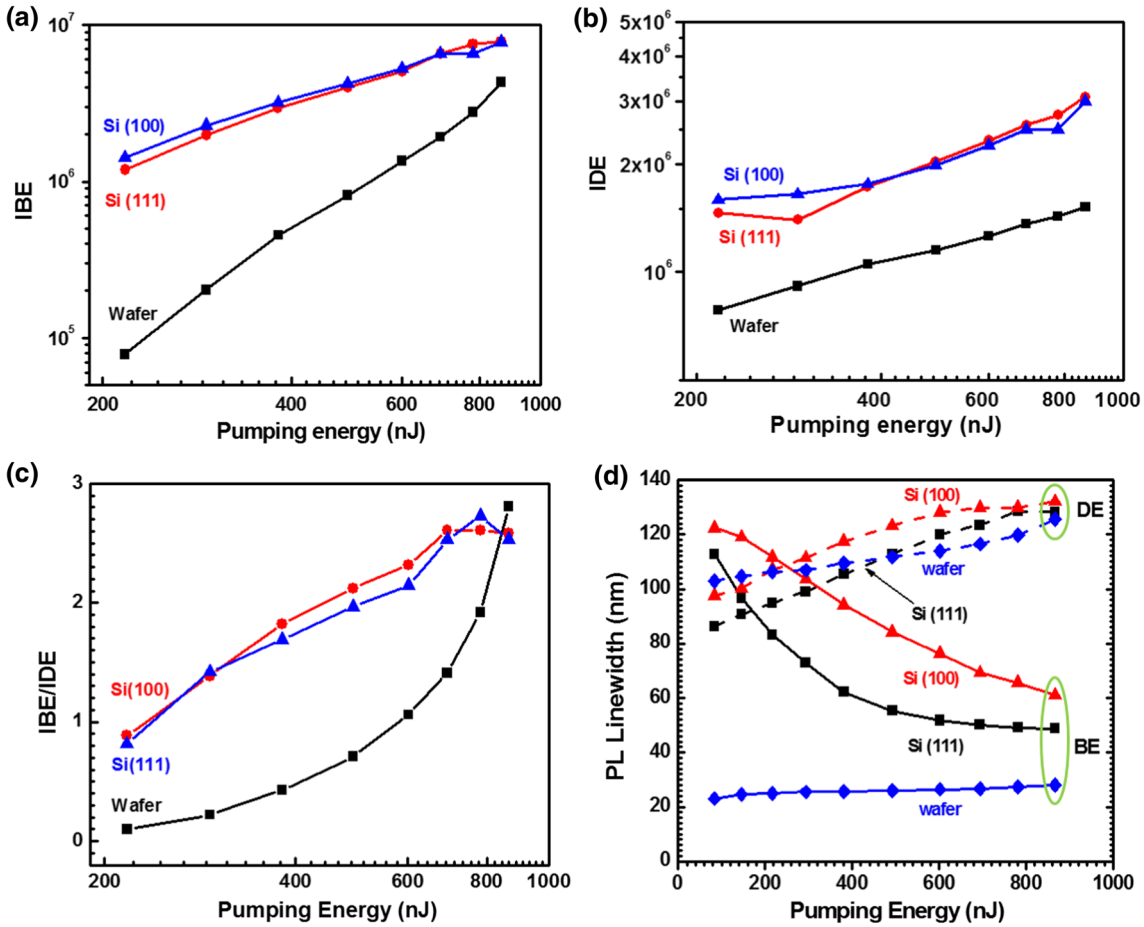

Fig. 6 Comparison of optical characteristics of GaP NWs grown on Si (111) and (100) (both at 800 °C for 15 min and 1–1.5 nm Au catalyst) and single crystal GaP under different laser pumping levels. **a** IBE, **b** IDE, **c** IBE/IDE ratio; and the linewidths of PL peaks (**d**)

tration of native defects that results in slight variation in DE peak position.

4 Conclusion

In summary, we presented an Au-catalyzed VLS strategy for the growth of highly stoichiometric GaP NWs on Si substrates with a simple low-cost CVD method. It was found that excess phosphorous precursor is necessary to restore the chemical balance in the air above the precursor boat, to inhibit the incongruent sublimation of P and Ga, and to finally lead to high quality nanowire product. As a result, highly stoichiometric GaP NWs are grown with less defects and stronger band edge emission. The sublimation behavior of these precursors was explained using the concept of chemical potential. This strategy and the associated understanding are established through a systematic growth study and characterization by comparing three sets of precursors: pure GaP, GaP + Ga, and GaP+P. From the structural study of NWs grown under P-rich condition the formation of coherent twin planes or TSLs as the structural defects in body of VLS-grown NWs was also noticed. The effect of growth parameters such as time, type of silicon substrate, growth temperature, etc., on suppression of DE caused by intrinsic crystal imperfections was demonstrated. Our comprehensive growth and characterization study allowed us to relate the growth conditions and the precursors to stoichiometry of NWs and the latter in turn to the existence and degree of deep defect states and band edge emission. Since types and concentration of defects are important as well as the relative intensity of bandage emission for optoelectronic devices, it is therefore imperative to study the crucial roles of growth parameters and conditions and to develop a growth strategy to minimize defect bands and maximize band edge emission. We believe that such a growth strategy is not only important for GaP, but also for other III–V compounds. However, there are more aspects of such growth yet to be explored for other III–V compounds to eventually optimize material properties and maximize the band edge emission.

Finally, we would like to make some concluding comments about device applications of the high-quality GaP, especially GaP nanowires. We have pointed out

certain device applications in the introduction part. We emphasize that GaP is closest lattice-matched to Silicon and the growth of high quality GaP nanowire on Si could lead to a wide range of silicon based applications of GaP such as widegap detectors and silicon based solar cells. Compared to other semiconductors, have been used as a photoelectrode for efficient water reduction and direct conversion of the of solar energy to fuels [77,78]. With the highest band gap among all semiconductors with a refractive index of $n > 3$ throughout entire visible range, GaP has great potential for making advanced visible and infrared photonic devices requiring high refractive index. [79] In a recent work by Trofimov, the Si-integrated Perovskite-GaP NW platform has been used to demonstrate visible-light tunable microlasers [80]. For photodetection application, the NWs offer unique advantage due to their geometrical structure that traps light and increases absorption. The high photosensitivity of NWs is also due to the large surface-to-volume ratio [81,82]. Having a wider band gap, GaP in form of NW can be applied as a suitable platform for making highly efficient photodetectors with a large photoresponses in visible and UV wavelength ranges [83–85]. This range can further be extended to near infrared region by embedding lower band gap energy materials [86]. We believe that highly stoichiometric GaP nanowires on Si could lead to improved devices for all these applications and may lead to more exploration of new devices in the future.

Supplementary information The online version contains supplementary material available at https://doi.org/10.1140/epjs/s11734-021-00388-3.

Acknowledgements This work was supported by Department of Energy (DOE) (award number DE-AR0000625, with Massachusetts Institute of Technology (MIT) as the prime). The authors acknowledge the use of facilities within the LeRoy Eyring Center for Solid State Science at Arizona State University, especially David Wright for his assistance with the CVD set-up and technical help and Dr. Sherry Chang for her help with HRTEM measurement of nanowires.

References

1. L.N. Quan, J.H. Kang, C.Z. Ning, Y. Peidong, Nanowires for photonics. Chem. Rev. **119**(15), 9153–9169 (2019)
2. C.Z. Ning, L. Dou, P.D. Yang, Bandgap engineering in semiconductor alloy nanomaterials with widely tunable compositions. Nat. Rev. Mater. **2**(12), 1–14 (2017)
3. E. Barrigón, M. Heurlin, Z. Bi, B. Monemar, L. Samuelson, Synthesis and applications of III–V nanowires. Chem. Rev. **119**(15), 9170–9220 (2019)
4. J. Wong-Leung, I. Yang, Z.Y. Li, S.K. Karuturi, L. Fu, H.H. Tan, J. Chennupati, Engineering III–V semiconductor nanowires for device applications. Adv. Mater. **32**, 1904359 (2020)
5. J.J. Tietjen, J.A. Amick, The preparation and properties of vapor-deposited epitaxial $GaAs_{1-x}P_x$ using arsine and phosphine. J. Electrochem. Soc. **113**, 724–728 (1966)
6. N. Kornienko, D.D. Whitmore, Y. Yu, S.R. Leone, P. Yang, Solution phase synthesis of indium gallium phosphide alloy nanowires. ACS Nano **9**(4), 3951–3960 (2015)
7. S.E.H. Amiri, P. Ranga, D.Y. Li, F. Fan, C.Z. Ning, Growth of InGaP alloy nanowires with widely tunable bandgaps on silicon substrates. In: *Lasers and Electro-Optics (CLEO), 2017 Conference on (pp. 1–2)*. IEEE (2017)
8. M.G. Craford, R.D. Dupuis, M. Feng, F.A. Kish, J. Laskar, 50th anniversary of the light-emitting diode (LED): an ultimate lamp [scanning the issue]. Proc. IEEE **101**(10), 2154–2157 (2013)
9. M. Feifel, T. Rachow, J. Benick, J. Ohlmann, S. Janz, M. Hermle, F. Dimroth, D. Lackner, Gallium phosphide window layer for silicon solar cells. IEEE J. Photovoltaics **6**(1), 384–390 (2016)
10. A. Standing, S. Assali, L. Gao, M.A. Verheijen, D. Van Dam, Y. Cui, P.H. Notten, J.E. Haverkort, E.P. Bakkers, Efficient water reduction with gallium phosphide nanowires. Nat. Commun. **6**, 7824 (2015)
11. W.S. Shi, Y.F. Zheng, N. Wang, C.S. Lee, S.T. Lee, Synthesis and microstructure of gallium phosphide nanowires. J. Vacuum Sci. Technol. B Microelectron. Nanometer Struct. Process. Meas. Phenomena **19**(4), 1115–1118 (2001)
12. S. Assali, I. Zardo, S. Plissard, D. Kriegner, M.A. Verheijen, G. Bauer, A. Meijerink, A. Belabbes, F. Bechstedt, J.E.M. Haverkort, E.P.A.M. Bakkers, Direct band gap wurtzite gallium phosphide nanowires. Nano Lett. **13**(4), 1559–1563 (2013)
13. J.P. Boulanger, R.R. Lapierre, Patterned gold-assisted growth of GaP nanowires on Si. Semicond. Sci. Technol. **27**(3), 035002 (2012)
14. C. Liu, J. Sun, J. Tang, P. Yang, Zn-doped p-type gallium phosphide nanowire photocathodes from a surfactant-free solution synthesis. Nano Lett. **12**(10), 5407–5411 (2012)
15. Z. Gu, M.P. Paranthaman, Z. Pan, Vapor-phase synthesis of gallium phosphide nanowires. Cryst. Growth Des. **9**(1), 525–527 (2008)
16. H.W. Seo, S.Y. Bae, J. Park, H. Yang, S. Kim, Synthesis of gallium phosphide nanowires via sublimation method. Chem. Commun. **21**, 2564–2565 (2002)
17. G. Shen, Y. Bando, D. Golberg, InP-GaP Bi-coaxial nanowires and amorphous GaP nanotubes. J. Phys. Chem. C **111**(9), 3665–3668 (2007)
18. S.C. Lyu, Y. Zhang, H. Ruh, H.J. Lee, C.J. Lee, Synthesis of high-purity GaP nanowires using a vapor deposition method. Chem. Phys. Lett. **367**(5–6), 717–722 (2003)
19. Q.L. Ye, R. Scheffler, J. Kumari, R. Leverenz, Growth and characterization of single crystalline InSb nanowires for thermoelectric applications (2007)
20. X. Yang, G. Wang, P. Slattery, J.Z. Zhang, Y. Li, Ultrasmall single-crystal indium antimonide nanowires. Crystal Growth Des. **10**(6), 2479–2482 (2010)
21. S. Vaddiraju, M.K. Sunkara, A.H. Chin, C.Z. Ning, G.R. Dholakia, M. Meyyappan, Synthesis of group III anti-

monide nanowires. J. Phys. Chem. C **111**(20), 7339–7347 (2007)
22. S.E. Hashemi Amiri, L. Gan, F. Fan, P. Ranga, C.Z. Ning, High-quality indium phosphide films and nanonetwork grown using low-cost metal-catalyzed vapor–liquid–solid method for photovoltaic applications. Adv. Opt. Mater. 1800136 (2018)
23. S.E.H. Amiri, S. Turkdogan, F. Fan, Y. Yu, P. Ranga, C.Z. Ning, Growth of stoichiometric InP nanowires/nanobelts by a facile vapor transport method. In: *CLEO: Science and Innovations (pp. SM1R-6)*. Optical Society of America (2016)
24. H. Wenzl, A. Dahlen, A. Fattah, S. Petersen, K. Mika, D. Henkel, Phase relations in GaAs crystal growth. J. Cryst. Growth **109**(1–4), 191–204 (1991)
25. C.T. Foxon, J.A. Harvey, B.A. Joyce, The evaporation of GaAs under equilibrium and non-equilibrium conditions using a modulated beam technique. J. Phys. Chem. Solids **34**(10), 1693–1701 (1973)
26. S.S. Matsuo, Properties of flash-evaporated gallium arsenide and gallium phosphide epitaxial films (1967)
27. C.E.C. Wood, K. Singer, T. Ohashi, L.R. Dawson, A.J. Noreika, A pragmatic approach to adatom-induced surface reconstruction of III-V compounds. J. Appl. Phys. **54**(5), 2732–2737 (1983)
28. M.H. Sun et al., Photoluminescence properties of InAs nanowires grown on GaAs and Si substrates. Nanotechnology **21**(33), 335705
29. J. Greenberg, *Thermodynamic basis of crystal growth: PTX phase equilibrium and non-stoichiometry*, vol. 44 (Springer Science & Business Media, Singapore, 2013)
30. V.P. Zlomanov, A.J. Zavrazhnov, A.V. Davydov, Nonstoichiometry and P-T-x diagrams of binary systems. Intermetallics **11**(11–12), 1287–1291 (2003)
31. U. Philipose, G. Sapkota, Defect formation in InSb nanowires and its effect on stoichiometry and carrier transport. J. Nanopart. Res. **15**(12), 2129 (2013)
32. P. Ranga, *Growth and Characterization of III-V Phosphide Nanowires* (Arizona State University, Tempe, 2016)
33. S.P. Lewis, M.L. Cohen, Electronic structure of nonstoichiometric Ga-As compounds. Mater. Sci. Eng. B **22**(2–3), 290–296 (1994)
34. G.G. Libowitz, Nonstoichiometry in chemical compounds. Prog. Solid State Chem. **2**, 216–264 (1965)
35. J.A. Van Vechten, Simple theoretical estimates of the enthalpy of antistructure pair formation and virtual-enthalpies of isolated antisite defects in zinc-blende and wurtzite type semiconductors. J. Electrochem. Soc. **122**(3), 423–429 (1975)
36. M.G. Craford, W.O. Groves, Vapor phase epitaxial materials for LED applications. Proc. IEEE **61**(7), 862–880 (1973)
37. H.A. Tahini, A. Chroneos, S.T. Murphy, U. Schwingenschlögl, R.W. Grimes, Vacancies and defect levels in III-V semiconductors. J. Appl. Phys. **114**(6), 063517 (2013)
38. A. Fazzio, L.M. Brescansin, J.R. Leite, Electronic structure of neutral and negatively charged gallium vacancies in GaP. J. Phys. C Solid State Phys. **15**(2), L1 (1982)
39. L. Wang, J.A. Wolk, L. Hsu, E.E. Haller, J.W. Erickson, M. Cardona, T. Ruf, J.P. Silveira, F. Briones, Gallium self-diffusion in gallium phosphide. Appl. Phys. Lett. **70**(14), 1831–1833 (1997)
40. A.S. Jordan, R. Caruso, A.R. Von Neida, M.E. Weiner, Solid composition and gallium and phosphorus vacancy concentration isobars for GaP. J. Appl. Phys. **45**(8), 3472–3476 (1974)
41. A. Höglund, C.W.M. Castleton, S. Mirbt, Relative concentration and structure of native defects in GaP. Phys. Rev. B **72**(19), 195213 (2005)
42. R.M. Sheetz, I. Ponomareva, E. Richter, A.N. Andriotis, M. Menon, Defect-induced optical absorption in the visible range in ZnO nanowires. Phys. Rev. B **80**(19), 195314 (2009)
43. U. Philipose, T. Xu, S. Yang, P. Sun, H.E. Ruda, Y.Q. Wang, K.L. Kavanagh, Enhancement of band edge luminescence in ZnSe nanowires. J. Appl. Phys. **100**(8), 084316 (2006)
44. H. Mori, M. Ogasawara, M. Yamamoto, M. Tachikawa, New hydride vapor phase epitaxy for GaP growth on Si. Appl. Phys. Lett. **51**(16), 1245–1247 (1987)
45. K. Park, J.A. Lee, H.S. Im, C.S. Jung, H.S. Kim, J. Park, C.L. Lee, GaP-ZnS pseudobinary alloy nanowires. Nano Lett. **14**(10), 5912–5919 (2014)
46. F. Rinaldi, Basics of molecular beam epitaxy (MBE). Annual Report, 1–8 (2002)
47. M.J. Mondry, E.J. Caine, H. Kroemer, A GaP decomposition source for producing a dimer phosphorus molecular beam free of gallium and tetramer phosphorus. J. Vacuum Sci. Technol. A Vacuum Surf. Films **3**(2), 316–318 (1985)
48. W.G. Schmidt, III-V compound semiconductor (001) surfaces. Appl. Phys. A **75**(1), 89–99 (2002)
49. H. Döscher, K. Möller, T. Hannappel, GaP (1 0 0) and InP (1 0 0) surface structures during preparation in a nitrogen ambient. J. Cryst. Growth **318**(1), 372–378 (2011)
50. H. Döscher et al., III–V on silicon: observation of gallium phosphide anti-phase disorder by low-energy electron microscopy. Surf. Sci. **605**(15–16), L38–L41 (2011)
51. D.C. Law, Y. Sun, R.F. Hicks, Reflectance difference spectroscopy of gallium phosphide (001) surfaces. J. Appl. Phys. **94**(9), 6175–6180 (2003)
52. C. Ratcliff et al., High temperature step-flow growth of gallium phosphide by molecular beam epitaxy and metalorganic chemical vapor deposition. Appl. Phys. Lett. **99**(14), 141905 (2011)
53. M.R. Leys et al., On the growth of gallium phosphide layers on gallium phosphide substrates by MOVPE. J. Electron. Mater. **18**(1), 25–31 (1989)
54. F.M. Davidson, R. Wiacek, B.A. Korgel, Supercritical fluid–liquid–solid synthesis of gallium phosphide nanowires. Chem. Mater. **17**(2), 230–233 (2005)
55. G. Job, F. Herrmann, Chemical potential–a quantity in search of recognition. Eur. J. Phys. **27**(2), 353 (2006)
56. G. Job, Allgemeines Grenzgesetz fur das Verhalten der Stoffe bei hoher Verdünnung Z̈. Physik. Chem. N. F. **87**, 113–24 (1973)
57. J.B. Wang, Z.F. Li, P.P. Chen, W. Lu, T. Yao, Raman study of gap mode and lattice disorder effect in InN films prepared by plasma-assisted molecular beam epitaxy. Acta Mater. **55**(1), 183–187 (2007)
58. A.S. Nasibov, N.N. Mel'nik, I.V. Ponomarev, S.V. Romanko, S.B. Topchıı, A.N. Obraztsov, MYu. Bashtanov, A.A. Krasnovskıı, Quantum Electron. **28**, 403 (1998)

59. Y. He, N.A. El-Masry, J. Ramdani, S.M. Bedair, T.L. McCormick, R.J. Nemanich, E.R. Weber, Determination of excess phosphorus in low-temperature GaP grown by gas source molecular beam epitaxy. Appl. Phys. Lett. **65**(13), 1671–1673 (1994)
60. K. Kuriyama, Y. Miyamoto, M. Okada, Redshift of the longitudinal optical phonon in neutron irradiated GaP. J. Appl. Phys. **85**(7), 3499–3502 (1999)
61. I.R. Lewis, H. Edwards, *Handbook of Raman spectroscopy: from the research laboratory to the process line* (CRC Press, New York, 2001)
62. A. Cantarero, Review on Raman scattering in semiconductor nanowires: I. Theory. J. Nanophotonics **7**(1), 071598–071598 (2013)
63. de la Chapelle, M. Lamy, H.X. Han, C.C. Tang, Raman scattering from GaP nanowires. Eur. Phys. J. B Condens. Matter Complex Syst. **46**(4), 507–513 (2005)
64. J. Wu, D. Zhang, Q. Lu, H.R. Gutierrez, P.C. Eklund, Polarized Raman scattering from single GaP nanowires. Phys. Rev. B **81**(16), 165415 (2010)
65. R. Gupta, Q. Xiong, G.D. Mahan, P.C. Eklund, Surface optical phonons in gallium phosphide nanowires. Nano Lett. **3**(12), 1745–1750 (2003)
66. K.W. Adu, Q. Xiong, H.R. Gutierrez, G. Chen, P.C. Eklund, Raman scattering as a probe of phonon confinement and surface optical modes in semiconducting nanowires. Appl. Phys. A **85**(3), 287 (2006)
67. I. Zardo, S. Conesa-Boj, F. Peiro, J.R. Morante, J. Arbiol, E. Uccelli, G. Abstreiter, A.F. i Morral, Raman spectroscopy of wurtzite and zinc-blende GaAs nanowires: polarization dependence, selection rules, and strain effects. Phys. Rev. B **80**(24), 245324 (2009)
68. Q. Xiong, J. Wang, P.C. Eklund, Coherent twinning phenomena: towards twinning superlattices in III-V semiconducting nanowires. Nano Lett. **6**(12), 2736–2742 (2006)
69. P. Caroff, K.A. Dick, J. Johansson, M.E. Messing, K. Deppert, L. Samuelson, Controlled polytypic and twin-plane superlattices in III-V nanowires. Nat. Nanotechnol. **4**(1), 50 (2009)
70. Z. Ikonic, G.P. Srivastava, J.C. Inkson, Optical properties of twinning superlattices in diamond-type and zinc-blende-type semiconductors. Phys. Rev. B **52**(19), 14078 (1995)
71. F. Fan, S. Turkdogan, Z. Liu, D. Shelhammer, C.Z. Ning, A monolithic white laser. Nat. Nanotechnol. **10**(9), 796–803 (2015)
72. Qilin Gu, B. Wang, Correlation between structural defects and optical properties of Cu_2O nanowires grown by thermal oxidation. arXiv preprint arXiv:1012.5338 (2010)
73. J. Lähnemann, U. Jahn, O. Brandt, T. Flissikowski, P. Dogan, H.T. Grahn, Luminescence associated with stacking faults in GaN. J. Phys. D Appl. Phys. **47**(42), 423001 (2014)
74. U. Philipose, S. Yang, T. Xu, H.E. Ruda, Origin of the red luminescence band in photoluminescence spectra of ZnSe nanowires. Appl. Phys. Lett. **90**(6), 063103 (2007)
75. M. Scheffler, J. Bernholc, N.O. Lipari, S.T. Pantelides, Electronic structure and identification of deep defects in GaP. Phys. Rev. B **29**(6), 3269 (1984)
76. W. Kohn, L.J. Sham, Self-consistent equations including exchange and correlation effects. Phys. Rev. **140**(4A), A1133 (1965)
77. C. Liu et al., Zn-doped p-type gallium phosphide nanowire photocathodes from a surfactant-free solution synthesis. Nano Lett. **12**(10), 5407–5411 (2012)
78. A. Standing, S. Assali, L. Gao, M.A. Verheijen, D. Van Dam, Y. Cui, E.P. Bakkers, Efficient water reduction with gallium phosphide nanowires. Nat. Commun. **6**(1), 1–7 (2015)
79. H. Emmer, C.T. Chen, R. Saive, Yu. Dennis Friedrich, A.A. Horie, A. Faraon, H.A. Atwater, Fabrication of single crystal gallium phosphide thin films on glass. Sci. Rep. **7**(1), 1–6 (2017)
80. P. Trofimov, A.P. Pushkarev, I.S. Sinev, V.V. Fedorov, S. Bruyere, A. Bolshakov, S.V. Makarov, Perovskite-gallium phosphide platform for reconfigurable visible-light nanophotonic chip. ACS Nano **14**(7), 8126–8134 (2020)
81. Xing Dai, Maria Tchernycheva, Cesare Soci, Compound semiconductor nanowire photodetectors, in *Semiconductors and Semimetals*, vol. 94, (Elsevier, Amsterdam, 2016), pp. 75–107
82. C. Soci et al., ZnO nanowire UV photodetectors with high internal gain. Nano Lett. **7**(4), 1003–1009 (2007)
83. P.E. Petersen, R.G. Schulze, Gallium phosphide photodetector having an as-grown surface and producing an output from radiation having energies of 2.2 eV to 3.8 eV. U.S. Patent No. 3,976,872. 24 (1976)
84. K. Park et al., Synthesis of polytypic gallium phosphide and gallium arsenide nanowires and their application as photodetectors. ACS Omega **4**(2), 3098–3104 (2019)
85. G. Chen et al., High performance rigid and flexible visible-light photodetectors based on aligned X (In, Ga) P nanowire arrays. J. Mater. Chem. C **2**(7), 1270–1277 (2014)
86. P. Kuyanov, S.A. McNamee, R.R. LaPierre, GaAs quantum dots in a GaP nanowire photodetector. Nanotechnology **29**(12), 124003 (2018)